The Role of Boundary Layer Processes in Limiting PV Homogenization

YANG ZHANG AND PETER H. STONE

EAPS, Massachusetts Institute of Technology, Cambridge, Massachusetts

AMY SOLOMON

CIRES Climate Diagnostics Center, Boulder, Colorado

(Manuscript received 4 August 2008, in final form 12 November 2008)

ABSTRACT

A β-plane multilevel quasigeostrophic channel model with interactive static stability and a simplified parameterization of atmospheric boundary layer physics is used to study the role of different boundary layer processes in eddy equilibration and their relative effect in maintaining the strong boundary layer potential vorticity (PV) gradient.

The model results show that vertical thermal diffusion, along with the surface heat exchange, is primarily responsible for limiting PV homogenization by baroclinic eddies in the boundary layer. Under fixed SST boundary conditions, these two processes act as the source of the mean flow baroclinicity in the lower levels and result in stronger eddy heat fluxes.

Reducing surface friction alone does not result in efficient elimination of the boundary layer PV gradient, but the equilibrium state temperature gradient is still largely influenced by surface friction and its response to changes in surface friction is not monotonic. In the regime of strong surface friction, with reduced poleward eddy heat flux, a strong temperature gradient is still retained. When the surface friction is sufficiently weak along with the stronger zonal wind, the critical level at the center of the jet drops below the surface. As a result, in the lower levels, the eddy heat flux forcing on the mean flow moves away from the center of the jet and the equilibrium state varies only slightly with the strength of the vertical momentum diffusion in the boundary layer.

1. Introduction

It is known from observational studies that the planetary boundary layer is characterized by turbulent momentum and heat transports and strong surface friction as well as heat exchange with the underlying surface. However, with the existence of large-scale baroclinic eddies in the extratropics, what determines the boundary layer thermal structure and how these boundary layer processes influence the eddy equilibration are still open questions.

To understand the role of baroclinic eddies in atmospheric circulation, several theories have been proposed. However, these theories either fail to work in the boundary layer or simply neglect the influence of boundary layer processes. The baroclinic adjustment theory (Stone 1978; Lindzen 1993; Gutowski 1985; Cehelsky and Tung 1991) proposes a tendency of baroclinic eddies to neutralize the mean flow, which requires sufficient mixing of interior potential vorticity (PV) and surface temperature. Stone and Nemet (1996) compared this theory with observations and found that the theory works only in the free troposphere and fails to work near the lower boundary in the extratropics. Kirk-Davidoff and Lindzen (2000), calculating the PV gradient from observations, obtained similar results. The observed strong meridional surface temperature gradients challenge the validity of this theory. Under the assumption that eddies mix potential vorticity and surface temperature diffusively and that the horizontal eddy diffusivity is essentially vertically uniform, Schneider (2004) obtained a relation between surface temperature gradient and the thermal stratification in the extratropics. However, as Schneider mentions in his paper, this relation is derived from an idealized model in which the vertical diffusion is not considered. The influence of boundary layer processes on his result is neglected.

Corresponding author address: Yang Zhang, Room 54-1717, MIT, 77 Massachusetts Ave., Cambridge, MA 02139.
E-mail: yangzh@mit.edu

DOI: 10.1175/2008JAS2914.1

© 2009 American Meteorological Society

Stone and Nemet (1996) and Zurita-Gotor and Lindzen (2007) attribute the lack of surface thermal homogenization to the boundary layer processes. However, the mechanism by which the boundary layer limits the baroclinic adjustment is still not clear. Swanson and Pierrehumbert (1997), through an observational study of the lower troposphere heat flux, find that surface heat flux and vertical thermal diffusion in the boundary layer damp temperature fluctuations in very short time scales and suggest that these boundary layer processes may prevent the surface temperature mixing by baroclinic eddies. Zurita and Lindzen (2001) and Zurita-Gotor and Lindzen (2004) suggest that for short Charney waves, which only need to mix the PV around the critical level to equilibrate, surface friction can limit their homogenization of the surface temperature gradient. They propose that surface friction, by reducing surface westerlies, can prevent the critical level dropping to the surface; thus, the temperature gradient near the surface cannot be efficiently mixed. Results from James (1987) and James and Gray (1986) imply another possible mechanism by which surface friction influences the boundary layer PV structure. They found that under weak surface friction, the strong barotropic shear of the zonal mean flow can reduce the growth rate of baroclinic eddies and suppress the eddy activity. This ''barotropic governor'' effect, as indicated in Robinson (1997) and Chen et al. (2007), may also play an important role during eddy equilibration. The questions that we try to answer in this paper, when all these boundary layer processes are included, are how do these mechanisms work together to influence the lower troposphere thermal structure and which is the dominant mechanism that causes the failure of baroclinic adjustment theory in the boundary layer.

In this study, we also discuss the equilibrium response of eddy activity to different boundary layer processes. For each individual boundary layer process, there exist at least two different ways that it can influence the eddy behavior. First, in terms of the eddy energy budget, the direct effect of boundary layer processes is a damping of eddy energies (Peixoto and Oort 1992). This is consistent with some studies of linear baroclinic instability and eddy life cycle. Card and Barcilon (1982) and Valdes and Hoskins (1988), by including the effects of surface friction as modeled by an Ekman layer, showed that the boundary layer leads to a reduction in instability. The eddy life cycle study of Branscome et al. (1989), comparing the maximum eddy heat flux reached during the life cycle in viscous and inviscid cases, also illustrated that the boundary layer acts as a damping for the eddy fluxes. On the other hand, during eddy equilibration, boundary layer processes also influence the mean flow thermal structure and modify the mean flow available potential energy (MAPE), which can further affect the eddy energy and eddy heat fluxes. For each boundary layer process, how these two effects compete is another focus of this study.

In this study, we use Solomon and Stone's (2001a) modified quasigeostrophic (QG) model with a simplified boundary layer parameterization to study the role of the boundary layer in eddy equilibration. In spite of its simplifications, a QG model is still a useful process model that captures the essential midlatitude dynamics. Indeed, baroclinic adjustment theory was initially proposed based on baroclinic instability using the QG concept. In our model, the governing equation is coupled with a static stability tendency equation so that we can get rid of the limitation of the QG model pointed out by Gutowski (1985) and Schneider (2004). Our model, as shown in Solomon and Stone (2001a,b), can simulate the midlatitude climate (e.g., the equilibrated state thermal structure, the distribution of eddy fluxes, the dominant eddy scale, and the spectral distribution of eddy kinetic energy) fairly well compared to observations.

Solomon (1997b) used this model but with a shorter channel length (5260 km) to study the influence of boundary layer processes on eddy equilibration. In her study, surface friction and surface heat flux, as well as vertical thermal and momentum diffusion, share the same parameters. She found that the boundary layer in general damps the mean flow adjustment. However, the mechanism through which different boundary layer processes modify the equilibrated states was not clear. Thus, in this study, we use different parameters for each boundary layer process and vary the value of each parameter to investigate their different roles in eddy equilibration. In addition, even though the dominant transient eddies in the midlatitudes are medium-scale eddies [approximately 4000–5000 km, as shown by Randel and Held (1991) and Solomon (1997a)], the short channel length may not be able to provide enough space for wave–wave interactions and the variation of eddy length scales. Thus, in this study we use a more realistic channel length (21 040 km) for our model.

Our model results illustrate the importance of the vertical thermal diffusion and the surface heat exchange in determining the lower-level thermal structure [as proposed by Swanson and Pierrehumbert (1997)] and show that vertical thermal diffusion is the dominant process that prevents PV homogenization in the boundary layer. Even though these two processes are sinks of eddy energies, they also act as a source of the lower-level mean flow baroclinicity. In equilibration, the indirect effect of these two processes dominates and results in stronger eddy heat fluxes. When varying the surface

friction, our model indicates a different scenario from that in James and Gray (1986). We find that in addition to changing the vertical distribution of the critical level (Zurita and Lindzen 2001), surface friction also changes the meridional distribution of the critical latitude and influences the meridional distribution of eddy forcing, which can modify the temperature distribution even over the whole troposphere. However, reducing surface friction alone does not result in efficient elimination of the boundary layer PV gradient.

This paper is organized as follows: Section 2 is a brief description of the model used in this study, section 3 demonstrates some features of the nonlinear equilibration of baroclinic eddies in our standard run and the sensitivity of our model to the individual boundary layer processes, and section 4 summarizes our model results and discusses the mechanisms behind these results.

2. Model setup

The model used in this study is a β-plane multilevel quasigeostrophic model with interactive static stability and a simplified parameterization of atmospheric boundary layer physics, similar to that of Solomon and Stone (2001a,b) (also see appendix A for the details of the model and the definition of each variable). The model has a channel length of 21 040 km and a channel width of 10 000 km. A rigid lid is added at the top as the boundary condition. The bottom of this model is an ocean surface with fixed surface temperature. This means we assume that the eddy adjustment time scale is much shorter than the adjustment time scale of the underlying surface, which is reasonable for an ocean surface, especially for the wintertime when the midlatitude ocean has a deep mixed layer. As we will see in our experiments, most of the adjustment to equilibrium occurs on a time scale of a month, which is short compared to the variation time scale of the ocean mixed layer.

The surface heat flux in our model is parameterized with the linearized bulk aerodynamic drag formula with drag coefficient C_{dt} representing the strength of the process. In the boundary layer, the turbulent vertical heat flux is parameterized with the vertical diffusive form, whose strength can be controlled by the diffusion coefficient μ_s. The surface friction and the turbulent momentum flux are parameterized in a similar way by using the drag coefficient C_{df} and diffusion coefficient μ_m.

3. Effect of boundary layer processes

To investigate the influence of each boundary layer process, as will be discussed in this section, four groups of sensitivity studies are carried out for comparison with the standard run. In these studies we only vary the value of one coefficient at a time and keep the coefficients representing the other boundary layer processes unchanged. The boundary layer coefficient values used in these experiments are listed in Table 1.

Except in sections 3b and 3e, in which we discuss the transient response of our model to the sudden variation of vertical thermal diffusion and surface friction, all the experiments discussed in this section start from the axisymmetric radiative–convective equilibrium (RCE) state. Small-amplitude perturbations in wavenumbers 1 to 9 are added to the mean flow at the initial moment. All the experiments are integrated for 1000 days and the equilibrated states are the states averaged over the last 400 days.

Our standard run is the experiment designed to simulate the current winter climate by choosing realistic values for the parameters, similar to the standard run in Solomon and Stone (2001a). The standard run simulates the midlatitude thermal structure reasonably well, with one jet and with eddy activities centered at the center of the channel. Wavenumbers 6 and 5 are the linearly most unstable waves for the initial state; in equilibration, wavenumbers 6, 5, and 4 are the dominant waves. Figure 1 shows the evolution of the energy exchange terms[1] and the dissipation terms for eddy kinetic energy (EKE) and eddy available potential energy (EPE). The dissipation of energy by FFT filter is negligible and not shown in the figure. During the equilibration, frictional dissipation is the largest sink for EKE, which is also the case in the real atmosphere (Oort and Peixoto 1983). Boundary layer thermal diffusion, together with diabatic forcing and vertical eddy heat flux, also acts to remove EPE during the whole evolution, especially in the equilibrium state, in which the magnitude of the thermal diffusion term is comparable to the $P_e \rightarrow K_e$ term. Thus, the direct effect of the boundary layer is a damping of eddy energies.

a. Vertical thermal diffusion

A study of the sensitivity of the equilibrated states to the vertical thermal diffusion was accomplished by varying

[1] The terms $P_e \rightarrow K_e$, $P_m \rightarrow P_e$, and $K_e \rightarrow K_m$ are energy fluxes that transfer energy, separately, from EPE to EKE, from MAPE to EPE, and from EKE to MKE. They are the QG form energy fluxes that are defined in Peixoto and Oort (1992, chapter 14), where $P_e \rightarrow K_e$ is proportional to the vertical eddy heat flux, $P_m \rightarrow P_e$ is proportional to the meridional eddy heat flux, and $K_e \rightarrow K_m$ is proportional to the meridional eddy momentum flux. The sign of these fluxes is defined as positive if the flux acts to transfer energy in the direction shown by the arrow.

TABLE 1. Values of the coefficients used in the experiments that investigate the model sensitivity to different boundary layer processes, and the zonal mean eddy heat fluxes at the center of the channel in the level where they have maximum amplitudes (around 850 hPa) in the equilibrated states in these experiments.

Run	μ_s (m^2 s^{-1})	μ_m (m^2 s^{-1})	C_{df} (m s^{-1})	C_{dt} (m s^{-1})	$\overline{[v^*T^*]}_{\max}$ (K m s^{-1})	$\overline{[\omega^*T^*]}_{\max}$ (K Pa s^{-1})
SD	5	5	0.03	0.03	16.8	−0.30
tcd0	5	5	0.03	0.00	10.6	−0.21
tcd1	5	5	0.03	0.01	16.4	−0.30
tcd2	5	5	0.03	0.06	19.8	−0.38
snu0	0	5	0.03	0.03	7.8	−0.11
snu1	2	5	0.03	0.03	16.5	−0.23
snu2	10	5	0.03	0.03	22.7	−0.42
fcd1	5	5	0.01	0.03	27.6	−0.30
fcd2	5	5	0.06	0.03	15.6	−0.30
xnu0	5	0	0.03	0.03	21.6	−0.32
xnu1	5	2	0.03	0.03	20.8	−0.32
xnu2	5	10	0.03	0.03	16.3	−0.29

μ_s in Eq. (A6), which represents the strength of turbulent heat flux in the boundary layer. Figure 2 displays how the equilibrium states vary with the values of μ_s.

From Fig. 2 we find that vertical thermal diffusion can largely suppress the mixing of lower-level potential vorticity. As shown in the plot of the PV gradient (Fig. 2c), in the standard run, the PV gradient at the center of the channel, consistent with observations, is less than β only around 700 hPa, with a large PV gradient near the tropopause and the surface. At the surface, there is a strong negative PV gradient, which is the model's version of the surface PV delta function. If we turn off this vertical thermal diffusion, in the equilibrium states PV is well homogenized from 600 to 850 hPa, and the surface negative PV gradient is also largely reduced compared with the initial state. The strength of the vertical thermal diffusion also modifies the PV distribution by making it less homogenized under stronger thermal diffusion.

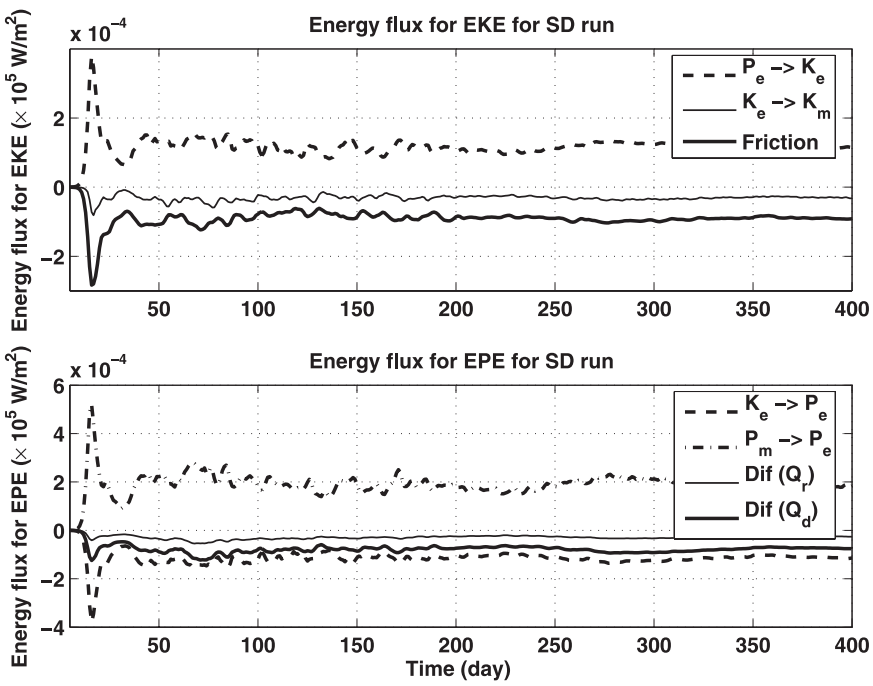

FIG. 1. Time series of energy flux terms (in 10^5 W m^{-2}) that can cause the variation of (top) EKE and (bottom) EPE in the first 400 days, where Dia(Q_r) in the lower figure is the damping of EPE by the diabatic heating Q_r and Dif(Q_d) is the damping of EPE by the thermal diffusion Q_d. Positive values indicate fluxes enhancing the energies; negative values indicate fluxes reducing the energies.

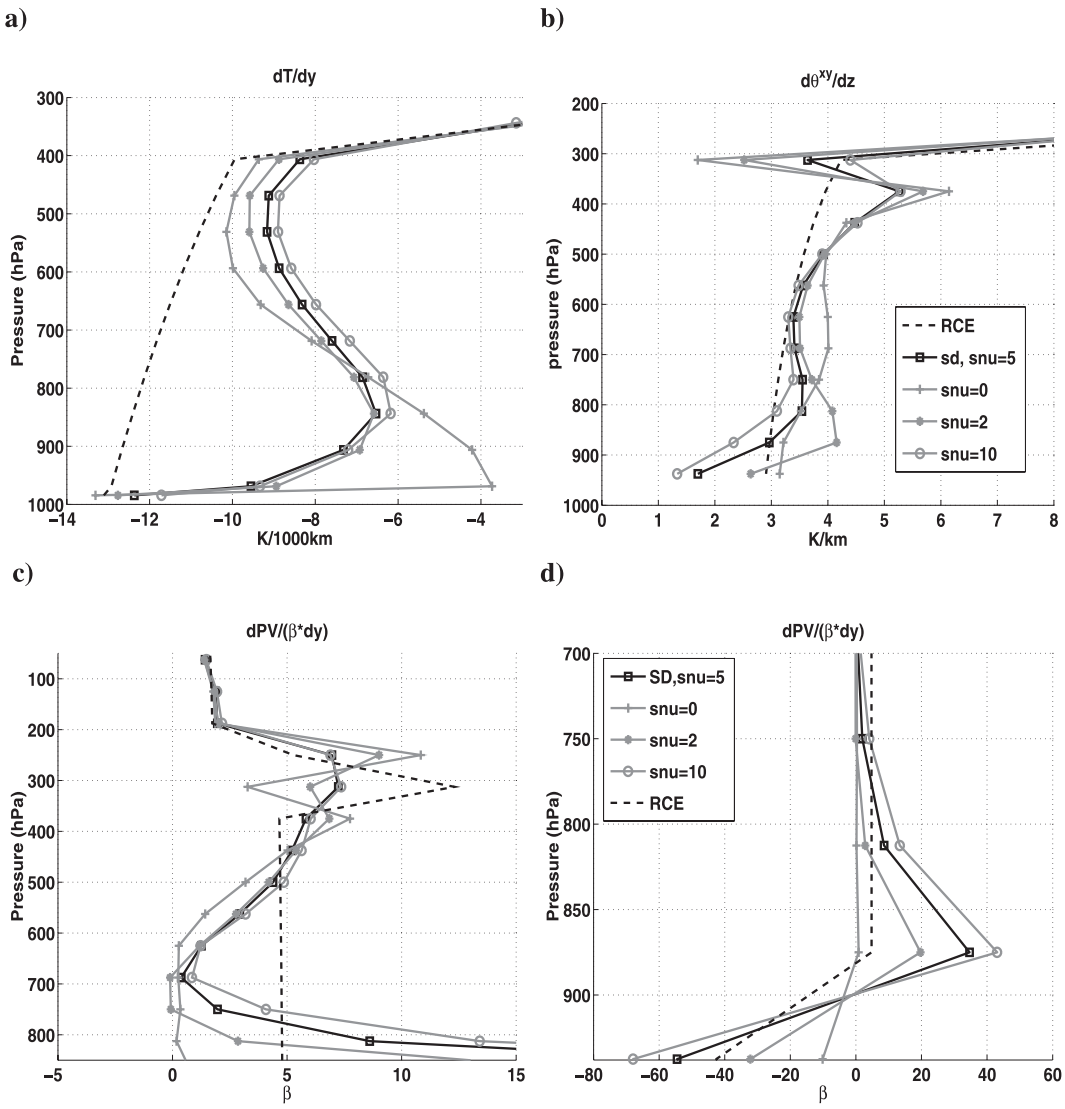

FIG. 2. Comparison of equilibrated state (a) zonal mean dT/dy at the center of the channel, (b) $d\overline{\theta}^{xy}/dz$, (c) zonal mean $dPV/(\beta dy)$ at the center in the free troposphere and (d) in the boundary layer for standard run (open square), the $\mu_s = 0$ (plus sign), 2 (asterisk), and 10 $m^2 s^{-1}$ runs (open circle) and the RCE state (black dashed curves).

Because in most of our experiments the baroclinic component dominates the PV gradient, the response of temperature gradients and static stability shows how the vertical thermal diffusion prevents the lower-level PV homogenization by influencing the thermal structure. When we turn off the vertical thermal diffusion, the zonal mean temperature distribution we obtain in the lower troposphere is very different from that in the standard run. As illustrated in Fig. 2a, the boundary layer temperature gradient is much stronger when vertical thermal diffusion is included. Because of the strong air–sea surface heat flux, the surface air temperature gradient almost keeps its initial value, which is also the prescribed temperature gradient of the underlying surface. The atmosphere above, without vertical thermal diffusion, is hardly coupled with the surface air, and its meridional temperature gradient is efficiently reduced primarily because of the mixing of baroclinic eddies. The static stability also behaves differently with and without thermal diffusion. Figure 2b shows that turning on the vertical thermal diffusion leads to a peak in the static stability near the top of the boundary layer (near 800 hPa), which is consistent with observations (Peixoto and Oort 1992). However, there is no such feature in the zero thermal diffusion case. This can be explained by looking back to Eq. (A1). Without thermal diffusion, the states of the boundary layer are determined by the balance between diabatic heating and vertical eddy heat flux.

However, with the thermal diffusion, the analysis of each term in Eq. (A1) in the equilibrium state shows that in the lower levels, diabatic heating is much smaller than the thermal diffusion and the eddy transports, and the balance is mainly between the latter two forcings.

Figure 2b illustrates that the strength of the vertical thermal diffusion can modify the static stability of the equilibrated mean states. Because the thermal diffusion is parameterized as being down the vertical temperature gradient, as shown in Fig. 2b, the increase in the thermal diffusion reduces the lower-level static stability. This is because the baroclinic eddies transport heat upward to stabilize the flow by cooling the lower troposphere and warming the upper troposphere. A stronger vertical turbulent heat flux in the lower levels can more efficiently compensate for the cooling by baroclinic eddies and prevent the stabilization of the flow.

The response of the eddy heat fluxes to the vertical thermal diffusion is different from what one might expect based on linear theories and life cycle studies. As displayed in Fig. 3, instead of acting as a damping, stronger vertical thermal diffusion results in enhanced eddy sensible heat fluxes. One phenomenon that helps us understand the response of the eddy heat fluxes and the importance of the vertical thermal diffusion, as well as other boundary layer processes, is the location of the critical level, which by definition is the level where zonal wind U is equal to the phase speed C_r. Figure 4 shows the cross section of the equilibrium state zonal wind and the intrinsic phase speed $(U - C_r)$ of the dominant wave, which is wavenumber 6 in these experiments, for the cases without thermal diffusion and with $\mu_s = 10\ \mathrm{m^2\ s^{-1}}$. The phase speeds of the dominant waves are calculated following Gall (1976):

$$C_r = [k(\phi_s^2 + \phi_c^2)]^{-1}\left(\phi_c \frac{\partial \phi_s}{\partial t} - \phi_s \frac{\partial \phi_c}{\partial t}\right), \qquad (1)$$

where k is the zonal wavenumber and ϕ_s and ϕ_c are the Fourier coefficients of the streamfunction. Consistent with the result that a larger temperature gradient is maintained with thermal diffusion, the jet is stronger for the $\mu_s = 10\ \mathrm{m^2\ s^{-1}}$ case. With the much weaker PV gradient for the non–thermal diffusion case, the critical level drops to 900 hPa. In the other case, the critical level lies near 800 hPa. If we think that the critical level for the baroclinic eddies generated by instability is their source level (Lindzen and Barker 1985), where the poleward eddy heat flux is largest according to the linear instability theory, then in all of these experiments the source region of the baroclinic eddies lies just inside the boundary layer or near the top of the boundary layer. The meridional eddy heat flux is collocated with the generation of baroclinic eddies and has a major component there. Thus, the role of the thermal diffusion, which always acts to keep the strong baroclinicity of the boundary layer and destabilize the lower-level flow, provides an explanation for the enhanced eddy heat fluxes.

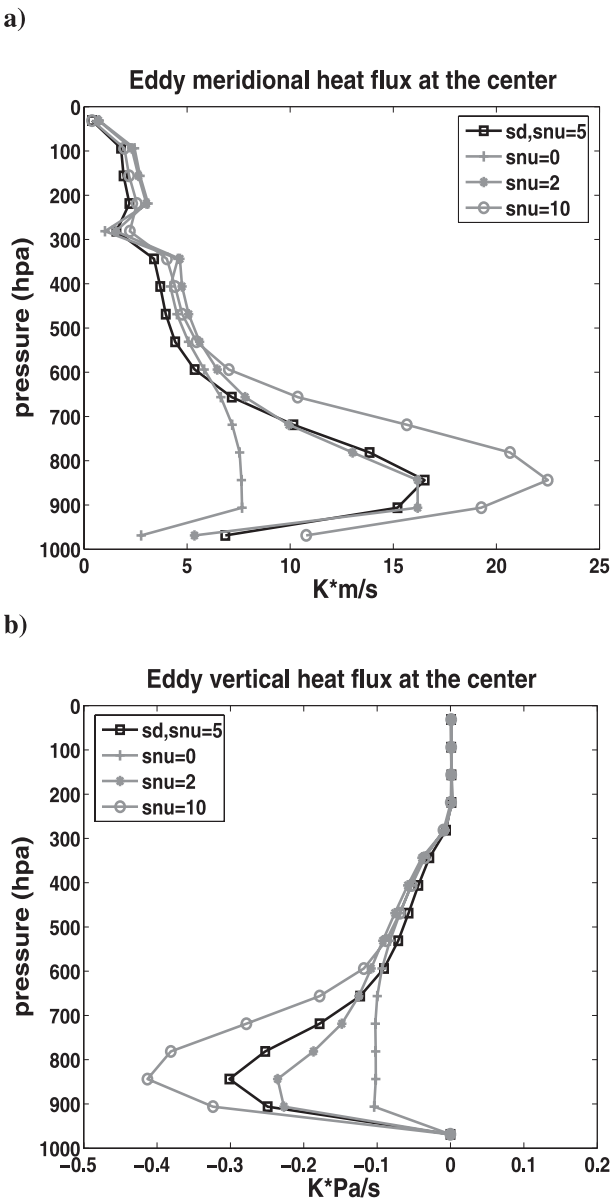

FIG. 3. Comparison of equilibrated state zonal mean (a) eddy meridional heat flux $[v^*T^*]$ and (b) eddy vertical heat flux $[\omega^*T^*]$, where [ ] indicates zonal mean, for the standard run (open square) and for the $\mu_s = 0$ (plus sign), 2 (asterisk), and 10 $\mathrm{m^2\ s^{-1}}$ runs (open circle).

b. *Transient response to vertical thermal diffusion*

To test the hypothesis we proposed above that explains the larger eddy heat fluxes as we increase the vertical

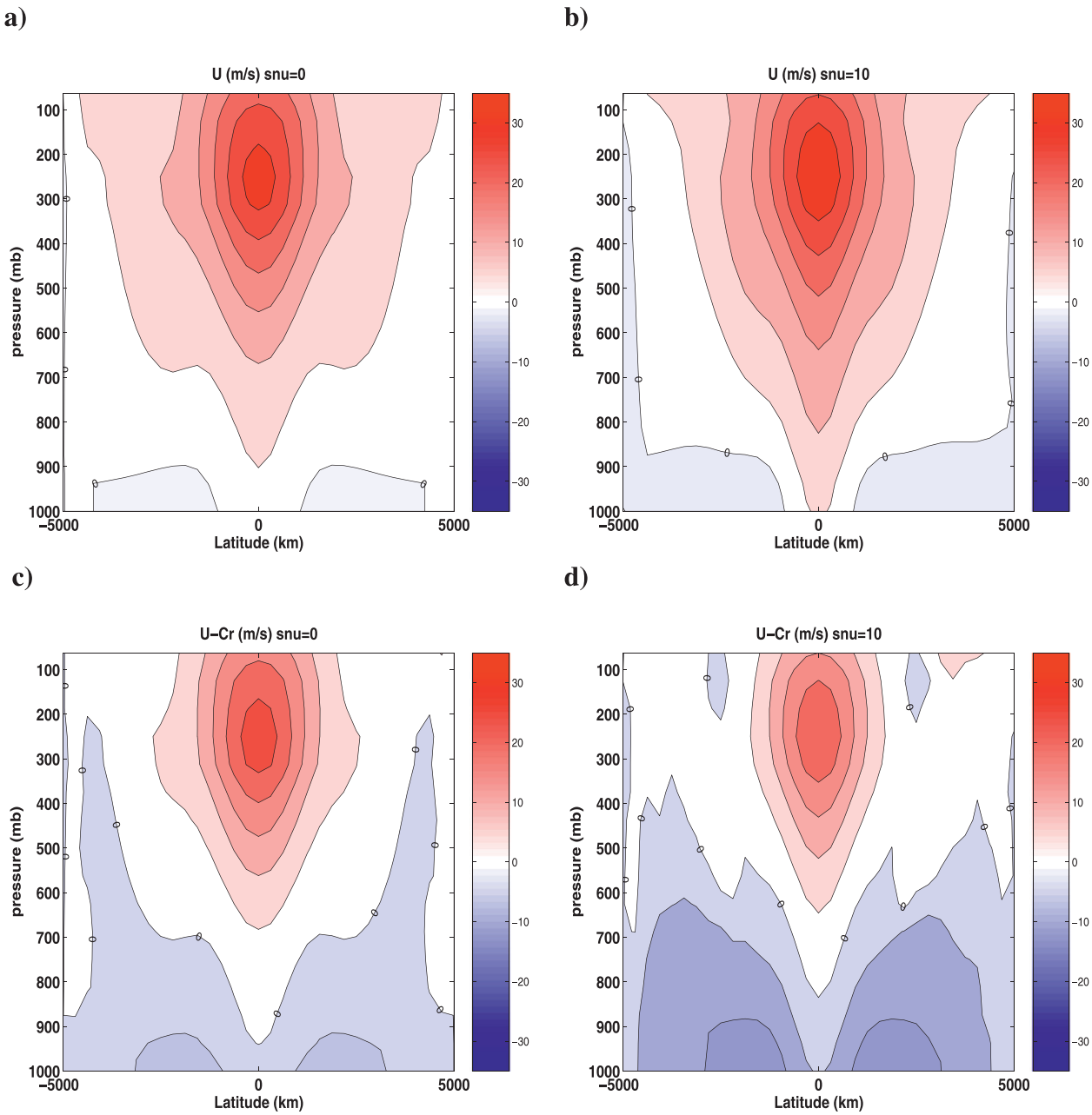

FIG. 4. (a),(b) Equilibrium state zonal wind for μ_s = (a) 0 and (b) 10 m^2 s^{-1} and (c),(d) intrinsic phase speed $U - C_r$ of the dominant wave for μ_s = (c) 0 and (d) 10 m^2 s^{-1}. The blue shaded region indicates negative value and the red shaded region indicates positive value; the contour interval is 5 m s^{-1} and the zero line is labeled.

thermal diffusion, a transient response study is carried out, in which the model starts from the equilibrium state of the standard run and a stronger vertical thermal diffusion (μ_s = 10 m^2 s^{-1}) is suddenly introduced. The response of the eddy heat fluxes and eddy energies to the sudden increase in μ_s is plotted in Fig. 5. We found that the immediate response of EPE and eddy heat fluxes is a decrease in their magnitude, which is consistent with the fact that vertical thermal diffusion is a damping term for EPE. However, the MAPE in the boundary layer increases quickly as we increase the thermal diffusion. Even though the MAPE in the free troposphere is almost unchanged, the total MAPE also increases immediately. Thus, after the initial decrease, both EPE and the eddy heat fluxes begin to increase. With several days' lag, EKE also starts to increase and

varies in close correlation with EPE. In the quasi-equilibrium state, MAPE and eddy heat fluxes all reach larger values, and EPE and EKE are marginally increased, primarily because of the compensating effect (i.e., stronger thermal diffusion also enhances the damping of eddy energies).

We also investigated the transient response of the flow to a sudden reduction of the vertical thermal diffusion, and we found the eddy behavior is just opposite to what we discussed above. EPE and eddy heat fluxes increase immediately as we reduce the thermal diffusion and then decrease gradually as the MAPE is reduced.

c. Surface heat flux

Because the ocean temperature is fixed in this experiment, the heat exchange between ocean and atmosphere acts to warm the surface air and the ocean surface behaves as an infinite source of heat. To study the influence of this surface heat flux, we vary the value of the heat exchange coefficient C_{dt} in Eq. (A4) and compare it with the standard run.

The equilibrated states for different C_{dt} are displayed in Fig. 6, from which we find that the surface temperature gradient strongly depends on this surface heat exchange. Without surface heat flux, the surface air temperature gradient is largely reduced. As C_{dt} increases, which indicates stronger heat exchange, the equilibrated surface air temperature gradient is forced to be closer to the temperature gradient of the underlying surface. Associated with this, the meridional eddy heat fluxes, as shown in Table 1, are enhanced for stronger surface heat flux.

Combining the results from the previous sensitivity experiments with vertical thermal diffusion, we find that surface air temperatures are mainly determined by the surface heat flux, and with the vertical thermal diffusion in the boundary layer, this surface air temperature gradient can further influence the interior baroclinic equilibration.

If we use the scale estimate to evaluate τ, the relaxation time scale of the surface air potential temperature to the surface heat flux forcing, from Eqs. (A4) and (A7),

$$\frac{\partial\theta}{\partial t} \sim \frac{g}{c_p}\frac{\partial F_{sh}}{\partial p},$$

$$\frac{\theta_{\mathrm{air}} - \theta_{\mathrm{sea}}}{\tau} \sim \frac{-g\, C_{dt}\rho_s(\theta_{\mathrm{air}} - \theta_{\mathrm{sea}})}{\Delta p}, \quad \text{and}$$

$$\tau \sim \frac{\Delta z}{C_{dt}},$$

and choose $\Delta z \approx 300$ m and $C_{dt} = 0.03$ m s^{-1} as realistic values, then the surface potential temperature relaxation time scale is 10^4 s, less than 1 day. This is consistent with the Swanson and Pierrehumbert (1997) study and confirms our numerical experiment results that the underlying surface temperature, through the surface heat flux, plays an important role in determining the equilibrium states. This time scale is much shorter than the relaxation time scale of the ocean mixed layer, which indicates that fixed ocean surface temperature is a reasonable approximation for this study.

d. Surface friction

Stronger[2] ($C_{df} = 0.06$ m s^{-1}) and weaker ($C_{df} = 0.01$ m s^{-1}) surface friction runs are carried out in this section to compare with the standard run. As displayed in Table 1, surface friction has a large influence on the meridional eddy heat flux. Weaker surface friction results in stronger meridional eddy heat flux. However, as shown in Fig. 7, the response of the equilibrated mean fields to the increasing surface friction is not monotonic. In the strong surface friction case, the temperature gradient at the center of the channel is reduced less through the whole troposphere than in the standard run. For weak surface friction, dT/dy is more reduced in the upper troposphere compared to the standard run, but not in the lower troposphere. The equilibrium PV gradient is not efficiently eliminated as we reduce the surface friction. Strong boundary layer PV gradients are observed in all the three runs. The PV gradient also displays a nonmonotonic tendency when reducing surface friction. Under weak surface friction, it is even stronger near 750 hPa than in the other two cases.

The spectral distribution of eddy kinetic energy (Figs. 8a–c) shows that enhancing the surface friction also affects the dominant wavelength in the equilibrium state. The dominant wavenumber (which is wavenumber 6 in the standard run) shifts to wavenumber 4 for $C_{df} = 0.01$ m s^{-1} and wavenumber 5 for the $C_{df} = 0.06$ m s^{-1} run. Such an effect is not found when varying the

[2] We use a stronger FFT filter in the fcd2 run, which makes the smallest eddy scale in the model 875 km instead of 750 km in the other numerical experiments discussed in this paper. We did so because of the numerical instability caused by the discontinuity of T_e across the tropopause. We find that when the larger-scale baroclinic eddies near the tropopause are too weak to smooth the sharp temperature discontinuity there, the smallest-scale eddies become active near the tropopause and our final states exhibit some unphysical features there, which can be eliminated by using a stronger FFT filter. By comparison, we find that using a stronger FFT filter only affects the equilibrium state near the tropopause and has no influence on the lower troposphere, and thus it does not affect the conclusions we make in this paper.

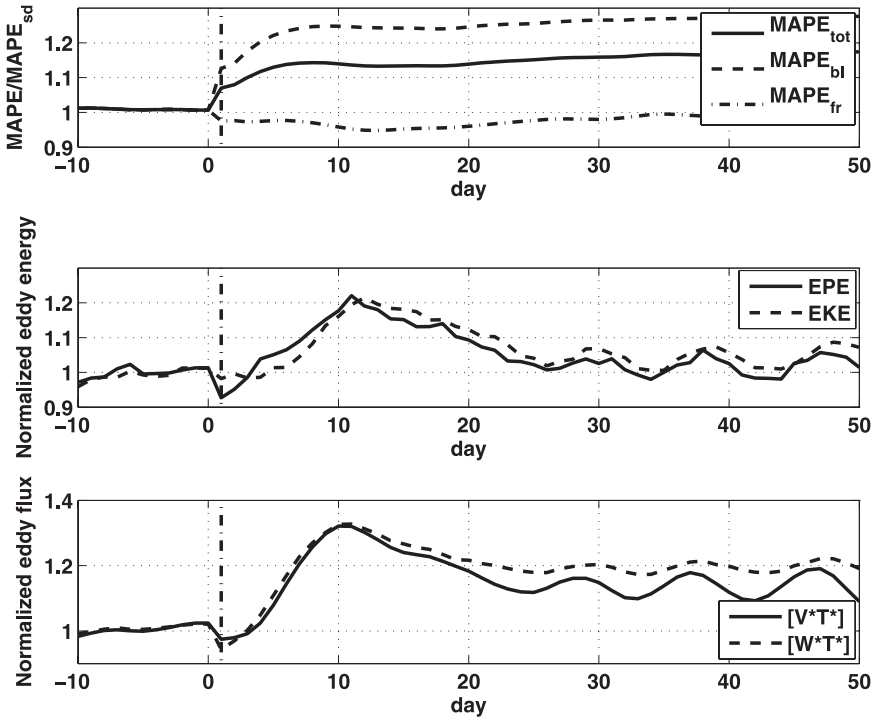

FIG. 5. Evolution of (top) normalized MAPE averaged globally, averaged over the boundary layer and the free troposphere, (middle) normalized EKE and EPE, and (bottom) normalized eddy meridional and vertical heat fluxes when the vertical thermal diffusion is suddenly increased at $t = 0$.

parameters representing the other boundary processes. Besides the dominant eddy scale, surface friction also affects the smaller-scale eddy spectral distribution, which implies that the enstrophy cascade and the inertial subrange are imperfect. Under weaker surface friction, the distribution is closer to the K^{-3} lines.

To understand the nonmonotonic response to the surface friction, the meridional distribution of the temperature differences between the equilibrium state and the initial state in the lower level (875 hPa) and the upper level (437.5 hPa) are plotted in Fig. 9, from which we find that baroclinic eddies reduce the temperature gradient by warming the poleward part of the flow and cooling the equatorward part of the flow. In both upper and lower levels, the magnitude of the temperature modification is larger for weaker surface friction, but the meridional distribution of the modification in the lower level is different as we vary the surface friction. When C_{df} is reduced to 0.01 m s^{-1}, the latitude of the strongest modification in the lower level moves away from the center of the channel. Thus, the temperature gradient is less reduced at the center of the channel but more modified in the flanking latitudes. In the upper levels, we find that the latitude of the maximum temperature modifications is unchanged in our experiments.

e. *Transient response to surface friction*

To understand the variation of the lower-level meridional distribution of the temperature modifications displayed in Fig. 9, we also study the transient response of the flow to the sudden reduction of the surface friction. We did an experiment that starts from the equilibrium state of the standard run and is forced by weaker surface friction (C_{df} = 0.01 m s^{-1}). After integrating the model for sufficiently long times, we obtain an equilibrium state (i.e., mean field and eddy heat fluxes) almost the same as the (C_{df} = 0.01 m s^{-1}) run in section 3d. The transient response of the lower-level flow is plotted in Fig. 10.

The domain-averaged EKE and EPE, as shown in Fig. 10a, grow immediately after reducing the surface friction. Through Fourier analysis, we find that the dominant wave scale switches from wavenumber 6 to wavenumber 4, which is consistent with the equilibrium run result. The meridional variation when reducing the surface friction in the lower level (875 hPa) is also displayed in Fig. 10, in which the direct response to the reduced surface friction is an acceleration of the lower-level zonal wind. Under weaker surface friction, as shown in Fig. 10c, a $U - C_r > 0$ region for the dominant wave appears, with the emerging critical latitudes moving away from the center of the channel. During days 10–20 the critical

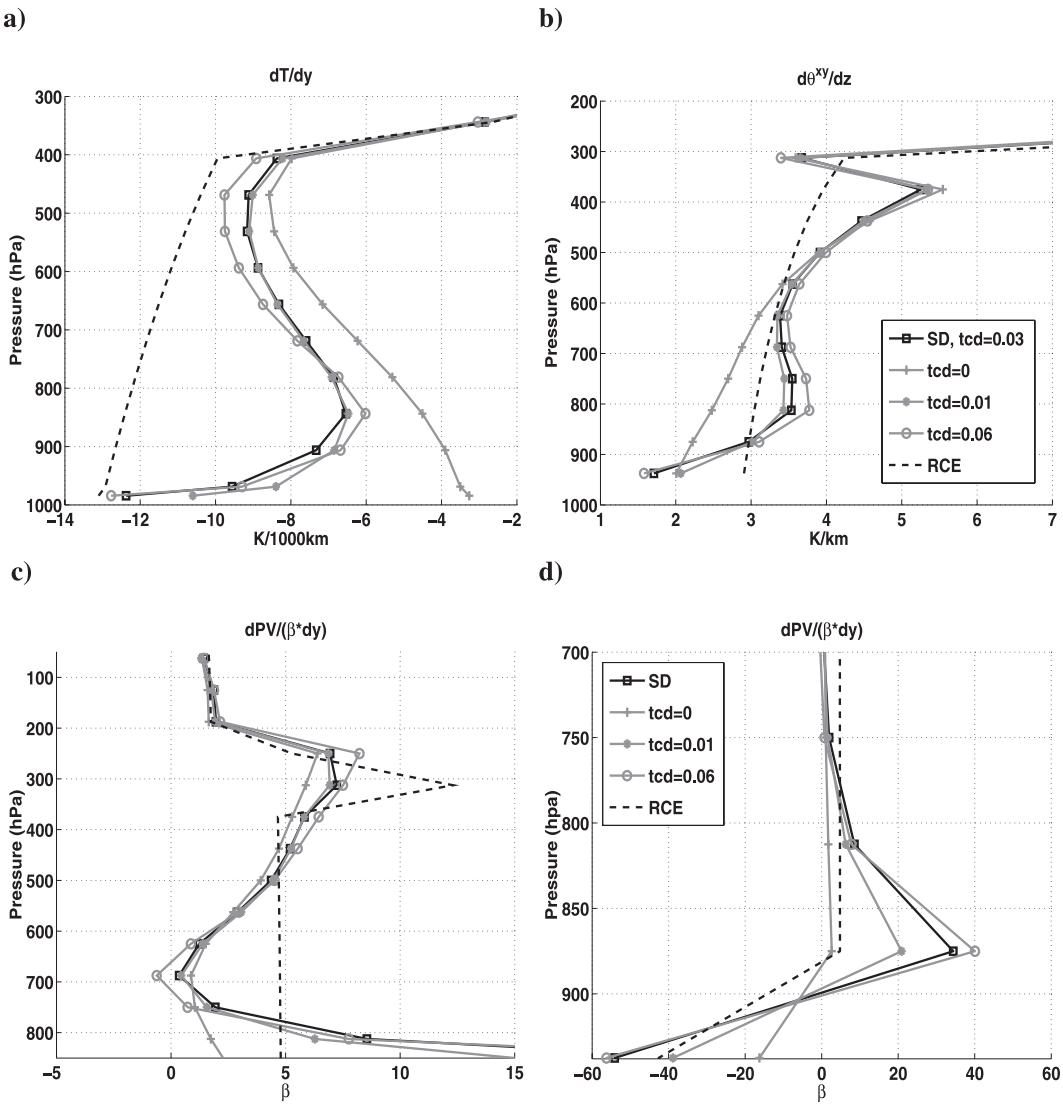

FIG. 6. Comparison of the equilibrated state (a) zonal mean dT/dy at the center of the channel; (b) $d\overline{\theta}^{xy}/dz$, (c) zonal mean $dPV/(\beta dy)$ at the center in the free troposphere; and (d) in the boundary layer for the standard run (open square), the $C_{dt} = 0$ (plus sign), 0.01 (asterisk), and 0.06 m s^{-1} runs (open circle), and the RCE state (black dashed curves).

latitudes reach their farthest location, which is around 1500 km away from the jet's center. The meridional distribution of $-\partial/\partial y[v^*T^*]$, which is the eddy forcing term in the thermodynamic equation (Holton 2004), is also displayed in Fig. 10c, in which the locations of the maximum eddy forcing also move away from the center of the channel and reach their farthest latitudes almost at the same time. The variation of the latitudinal distribution of the maximum eddy forcing is well correlated to the variation of critical latitudes. The latitudes at which temperature is most modified compared to the RCE state, as shown in Fig. 10d, evolve in the same pattern as the eddy forcing, which is consistent with what we have found in Fig. 9.

Our above transient response study implies a critical latitude–eddy forcing mechanism in our model. If we go back to our equilibrium runs in section 3d, we find that the distributions of lower-level eddy forcing and critical latitudes in the equilibrium states under different surface friction, as shown in Fig. 8, are consistent with this mechanism.

Figures 8d–f show that the change of the meridional distribution of the temperature modifications is closely related to the meridional distribution of eddy forcing $-\partial/\partial y[v^*T^*]$. As we increase the surface friction, the eddy forcing becomes weaker but still keeps a similar meridional distribution. However, when the surface friction is sufficiently weak, the position of the maximum forcing in the lower levels shifts away from the center of

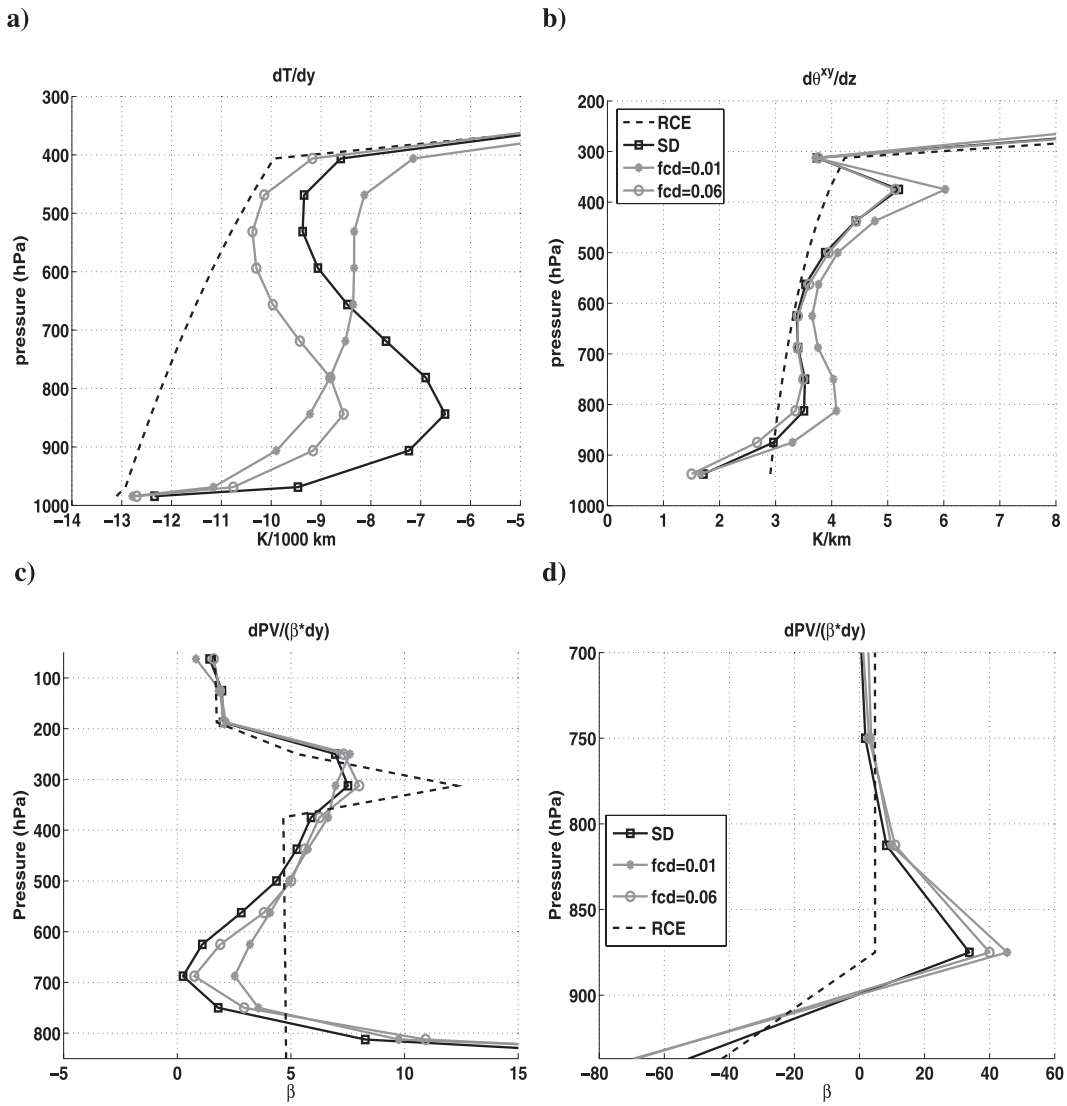

FIG. 7. As in Fig. 6, but for the standard run (open square), the $C_{df} = 0.01$ (asterisk) and 0.06 m s^{-1} runs (open circle), and the RCE state (black dashed curves).

the channel, and the eddy forcing at the center becomes weaker.

The structures of the zonal wind (Figs. 8g–i) and the distributions of $U - C_r$ for the dominant wave in the equilibrium state (Figs. 8j–l)[3] illustrate that even though under stronger surface friction the lower-level westerly and easterly wind bands become weaker, nonetheless the distribution of $U - C_r$ has a structure similar to that of the standard run. In both cases, the critical levels are near 800 hPa, which, as suggested by Lindzen and Barker (1985) and Simmons and Hoskins (1978), indicates that the eddies in the lower levels cannot propagate as waves and are dissipated in their source latitude. However, when the surface friction is sufficiently weak, the jet in the lower level becomes stronger and (as shown in appendix B) the dominant eddy scale becomes larger, with a smaller phase speed. Thus, the critical level drops to the surface. This allows the eddies in the lower levels to propagate away from the center of the channel, and the location of the wave absorption in the lower levels could move away from the center.

We also want to point out that as we reduce the surface friction, as displayed in Figs. 8h and 10b, the barotropic

[3] As shown in Fig. 8a, wavenumber 4 is the second most important component in maintaining the equilibrium state, whose distribution of $U - C_r$ is in the same pattern as wavenumber 6, and the critical level in the eddy source latitudes is also near 800 hPa.

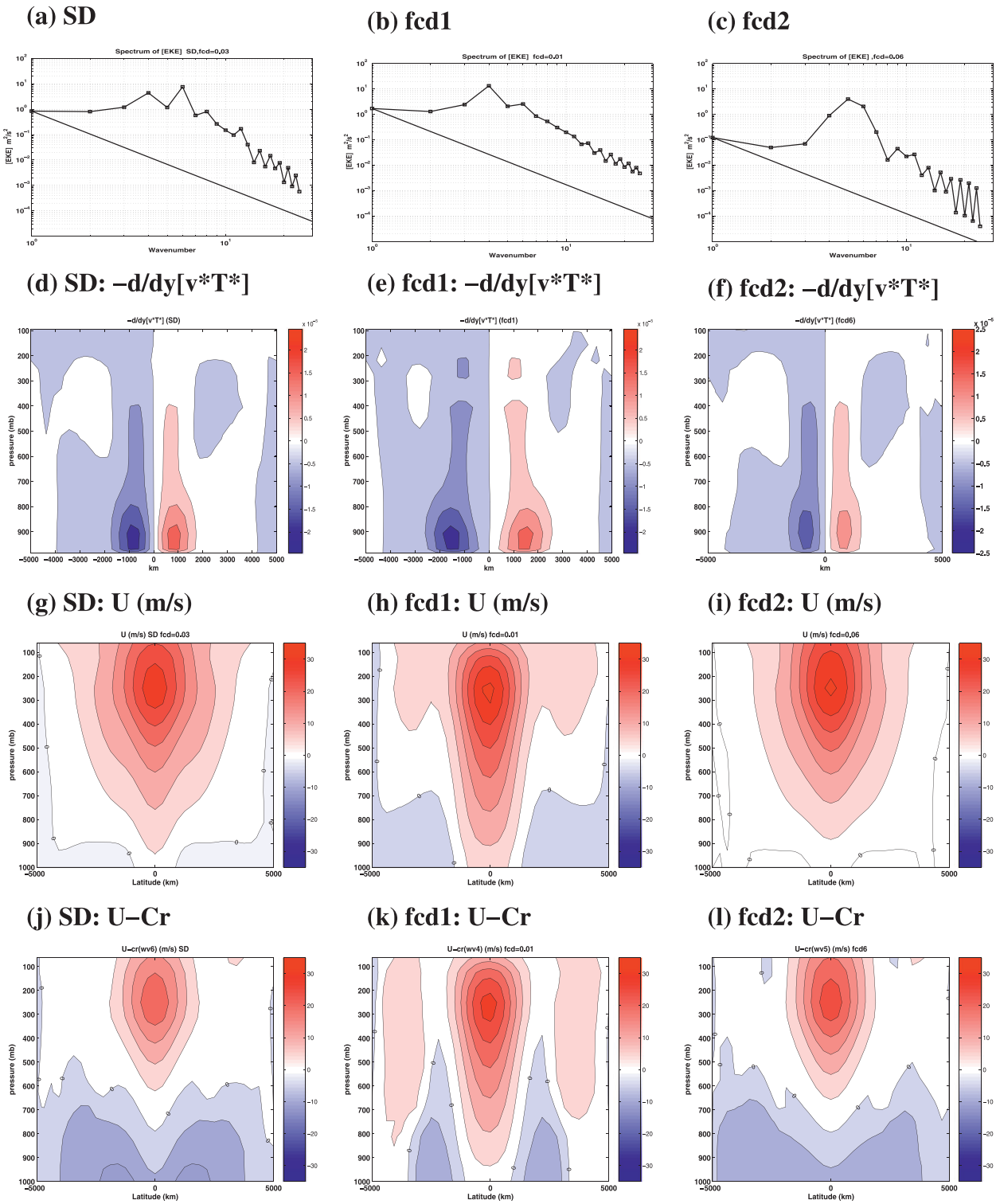

FIG. 8. Spectral distribution of the (a)–(c) equilibrium state EKE, where the straight line denotes the k^{-3} power law and (d)–(l) the cross sections of the equilibrium state convergence of (d)–(f) the meridional eddy heat flux $-d/dy[v^*T^*]$, (g)–(i) zonal wind, and (j)–(l) intrinsic phase speed $U - C_r$ of the dominant waves for the standard run and the $C_{df} = 0.01$ and 0.06 m s^{-1} runs, respectively. The contour interval for U and $U - C_r$ is 5 m s^{-1}, and the zero line is labeled. The blue shaded region indicates negative values (easterlies).

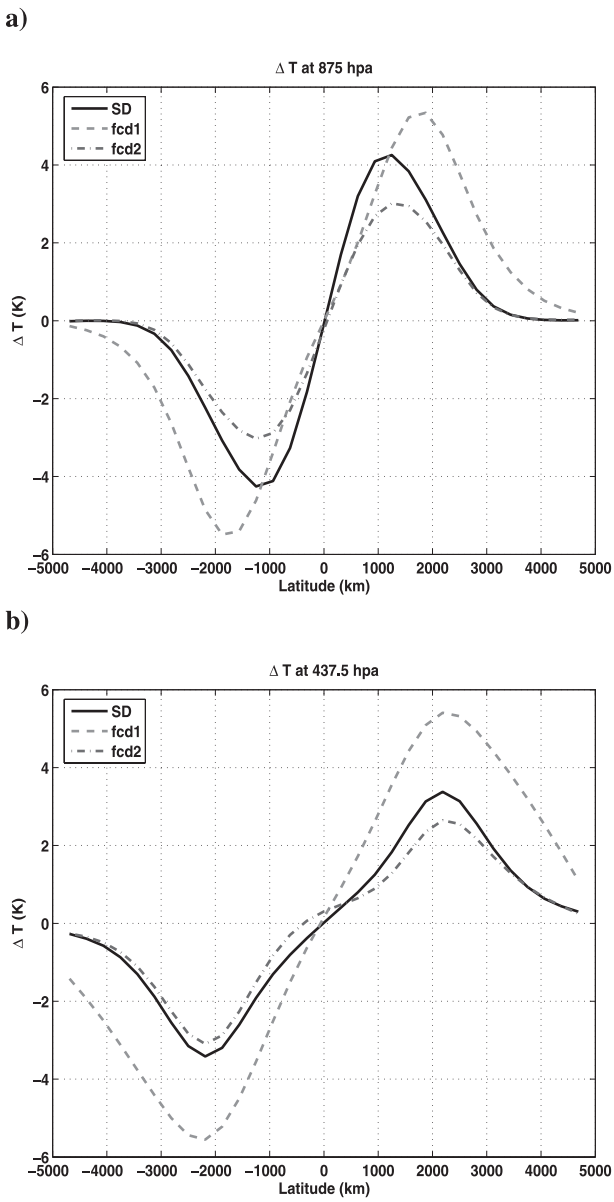

FIG. 9. Difference of temperature between equilibrium state and RCE (initial) state for the standard run (solid curves) and for the C_{df} = 0.01 (dashed curves) and 0.06 m s^{-1} runs (dotted–dashed curves) at (a) 875 and (b) 437.5 hPa.

shear also becomes stronger. The barotropic decay term in the energy cycle also becomes stronger, which can partly compensate the reduction of frictional dissipation for the eddy energy budget. However, in contrast to James and Gray (1986) and James (1987), the net result of reducing surface friction in our simulation is an increase of eddy energies as well as of eddy heat fluxes for most of the parameter regime. The barotropic governor effect is not the dominant mechanism that helps maintain the strong temperature gradient at the center of the channel.

f. Vertical momentum dissipation

The effect of the turbulent vertical momentum transport in the boundary layer is also studied by keeping all the other parameters unchanged and varying the coefficient μ_m in Eq. (A9). Compared with the standard run, as shown in Fig. 11, the vertical momentum dissipation in the boundary layer has little influence on the equilibrium states. The static stability is almost insensitive to the intensity of the momentum dissipation, and only the lower-level temperature gradient is slightly larger for the week momentum dissipation case. The influence of the momentum dissipation is weak on the PV gradient, too. Vertical momentum dissipation damps the eddy heat fluxes slightly.

4. Summary and discussion

In this work, by studying each of the boundary layer processes, we have investigated their different roles in eddy equilibration. Our results show that vertical thermal diffusion, along with the surface heat flux, is the dominant process that prevents the homogenization of the potential vorticity in the boundary layer, which provides an explanation for why the baroclinic adjustment theory fails to work there. When we include these two processes in the model as suggested by Swanson and Pierrehumbert (1997), we find that the surface heat flux is the dominant factor that determines the surface air temperature gradient. Vertical thermal diffusion couples the boundary layer, even the atmosphere above the boundary layer, with the surface air, so that the flow in the boundary layer can "feel" the strong temperature gradient at the surface. Thus, even though the surface temperature mixing by the baroclinic eddies is strong, the thermal diffusion can efficiently damp the temperature changes, and the lower levels' temperature gradient cannot be greatly reduced. Therefore, by keeping the strong surface temperature gradient as well as by preventing the stabilization of the boundary layer by baroclinic eddies, the vertical thermal diffusion modifies the slope of isentropes in the lower levels and suppresses the PV mixing.

The boundary layer vertical thermal diffusion and the surface heat flux act in general as a damping of the modification of the mean fields by baroclinic eddies. However, this is not a damping for the eddy heat fluxes. Instead, stronger thermal diffusion in our model results in stronger eddy heat fluxes. This tendency is not inconsistent with the previous linear instability studies and the eddy life cycle study by Branscome et al. (1989). As shown in Table 2, the maximum EKE and poleward eddy heat flux reached in the first eddy life cycle are also reduced when including the surface heat flux. As shown in section 2b, the immediate response of EPE and

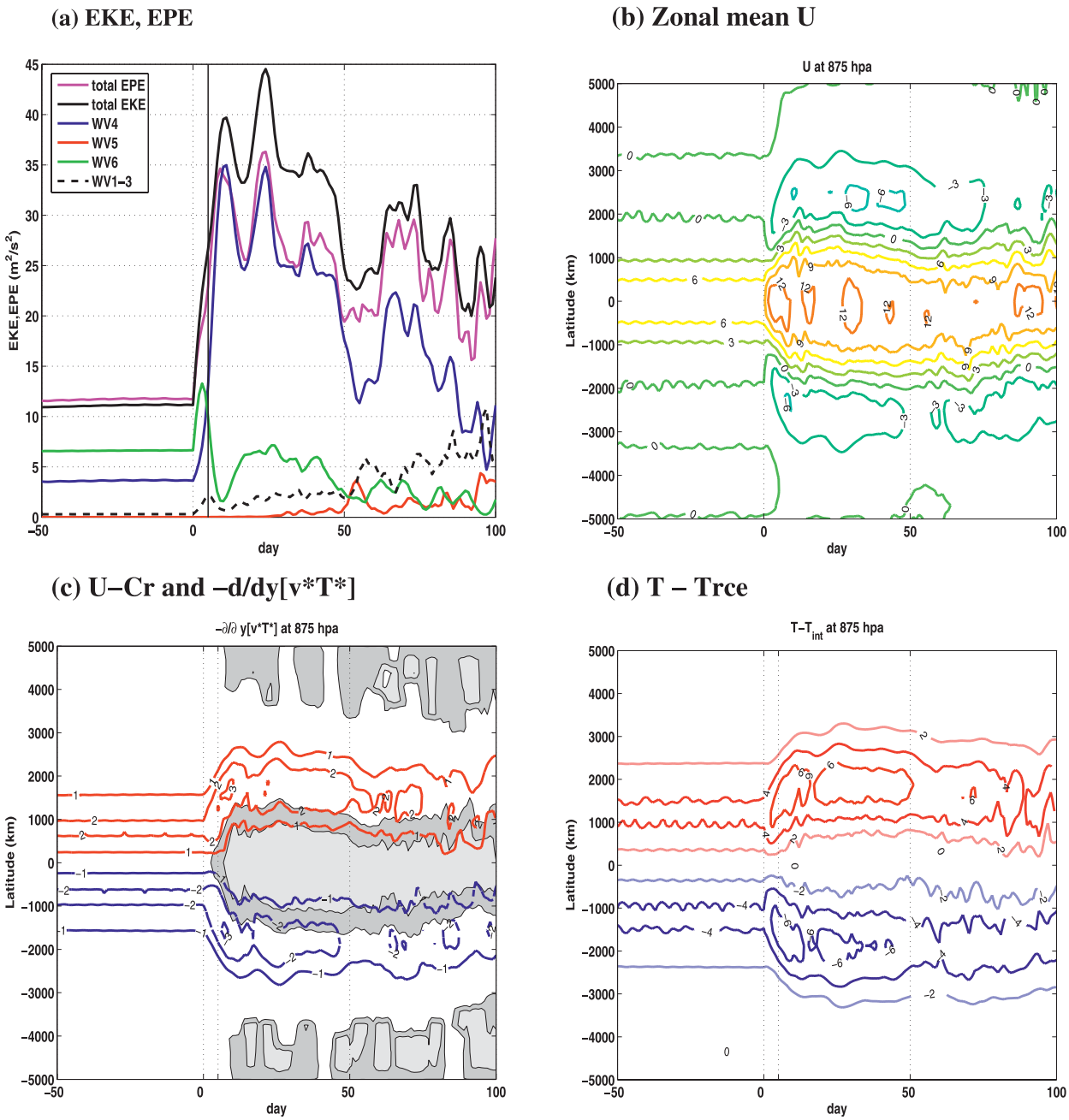

FIG. 10. Evolution of (a) total EKE (black curve) and EKE from wavenumbers 4 (blue curve), 5 (red curve), 6 (green curve) and 1–3, and the response of 875-hPa (b) zonal mean zonal wind, (c) $U - C_r$ (shaded) of the dominant wave and $-\partial/\partial y[v^*T^*]$ (contour), and (d) the temperature modification compared to the RCE state $T - T_{\mathrm{RCE}}$ to the reduced surface friction. Curve interval is 3 m s^{-1} for the zonal wind, 1.0×10^{-5} K s^{-1} for $-\partial/\partial y[v^*T^*]$, and 2 K for $T - T_{\mathrm{RCE}}$. For $U - C_r$, the shaded region is the area where $U - C_r > 0$; the contours plotted are 0, 5, and 10 m s^{-1}; and the thin dashed straight line shows the day when the dominant wave becomes wavenumber 4.

eddy heat fluxes to increased vertical thermal diffusion is still a decrease in their magnitude. However, in equilibrium, there exist two competing effects that influence the eddy behavior. The direct effect is that (consistent with the eddy life cycle study) the boundary layer thermal diffusion is always a damping term for eddy energies. On the other hand, it can also modify the mean flow and maintain the mean flow available energy, which is the energy source of baroclinic eddies and can further affect the eddy activity. In equilibrium, this indirect effect on eddies dominates the direct effect, resulting in stronger eddy heat fluxes.

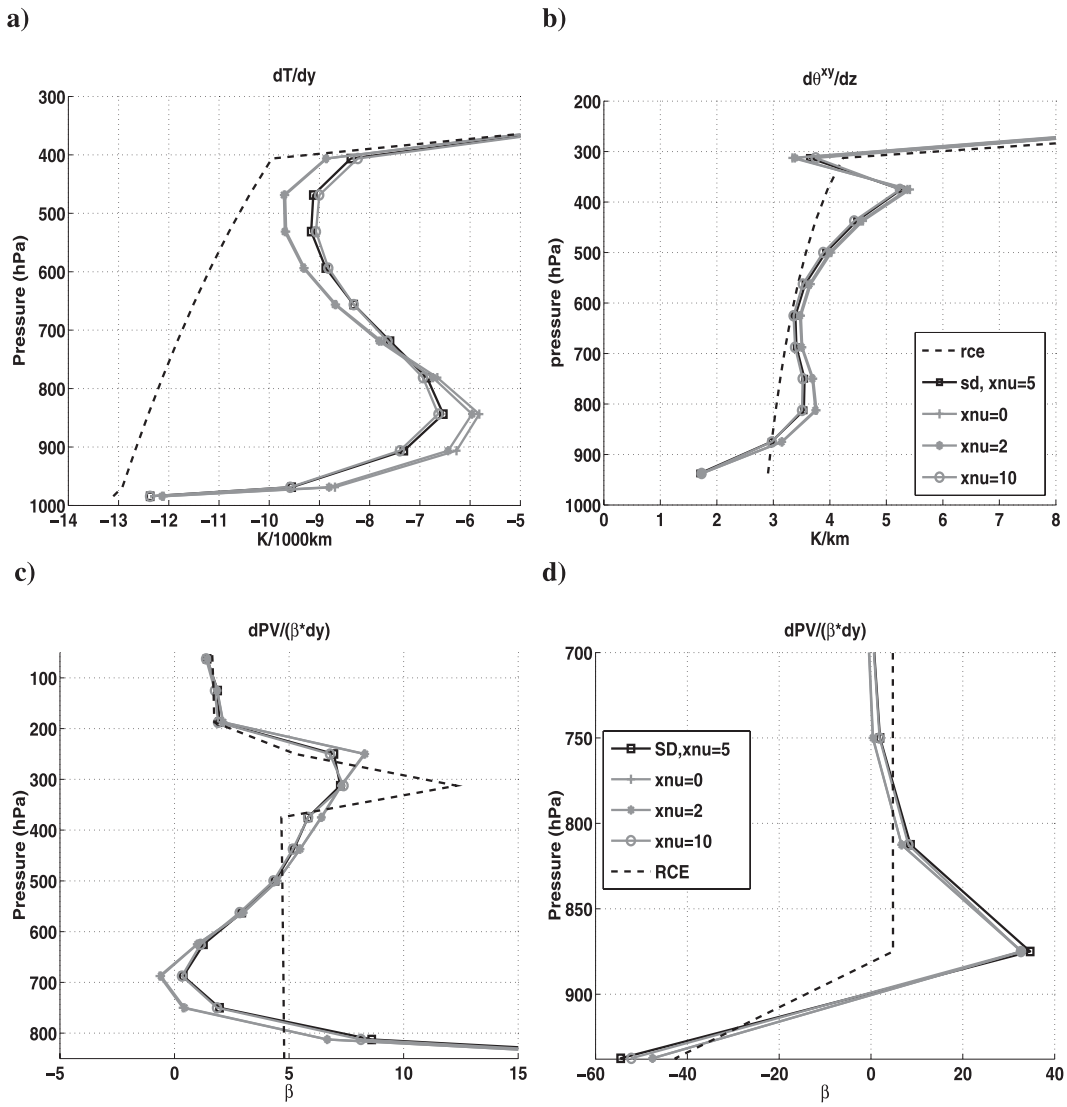

FIG. 11. As in Fig. 6, but for the standard run (open square) and for the $\mu_m = 0$ (plus sign), 2 (asterisk), and 10 $m^2\ s^{-1}$ runs (open circle) and the RCE state (black dashed curves).

In our study, the equilibrated states vary only slightly with the vertical momentum diffusion, but the meridional temperature gradient displays a large sensitivity to the surface friction. The mechanism through which surface friction modifies the equilibrated states is more complicated. First, our model shows that surface friction always acts as a damping of eddy activity. It reduces EKE as well as the magnitude of poleward eddy heat flux. In the regime of strong surface friction, this reduced eddy heat flux indicates a weaker eddy forcing and the temperature gradient is not reduced as much. On the other hand, surface friction also modifies the mean flow and influences the eddy length scale (a phenomenon that could be suppressed in the short channel). These two effects can further influence the distribution of the critical level. In the weak surface friction regime in our model, the lower-level zonal wind becomes stronger. The eddy length scale becomes larger and has a smaller phase speed (as shown in appendix B).

TABLE 2. Maximum EKE, EPE, and poleward eddy heat flux reached at the center of the channel during the first eddy life cycle. Energy is expressed as domain averaged energy density. Eddy heat flux is vertical averaged.

Run	C_{dt} ($m\ s^{-1}$)	EKE ($m^2\ s^{-2}$)	EPE ($m^2\ s^{-2}$)	$[v^*T^*]$ ($K\ m\ s^{-1}$)
SD	0.03	23	21	26.5
tcd0	0.00	35	30	31.6
tcd1	0.01	25	22	28.1
tcd2	0.06	22	19	25.3

Thus, the critical level in the source latitude drops below the surface and critical latitudes emerge in the lower levels. If eddies are more likely to propagate in the region of $U > C_r$, this implies that eddies in the lower levels are absorbed less near the center but more near the critical latitudes, which changes the meridional distribution of the eddy forcing. In this case, the temperature gradient in the lower levels at the center of the channel is not reduced efficiently.

Although the critical level of the dominant wave drops below the surface under weak surface friction [as suggested by Zurita and Lindzen (2001)], reducing surface friction alone does not result in efficient elimination of the boundary layer PV gradient. The strong boundary layer thermal damping still maintains the strong surface temperature gradient. Instead, the temperature gradient in the lower level is more related to the variation of the critical latitudes.

To conclude this study, our model results have shown that boundary layer processes play important roles in baroclinic eddy equilibration. This is especially true for the vertical thermal diffusion and the surface heat exchange, which are traditionally neglected or not well considered in the theoretical study of baroclinic eddies and in many atmospheric dynamic models [e.g., James and Gray (1986) and Held and Suarez (1994), as well as many recent studies using Held and Suarez's model]. The surface heat flux in the real atmosphere can act on the atmosphere with a shorter time scale than the baroclinic eddies. More important, the turbulent vertical heat transport in the boundary layer always acts to reduce the stratification, which is a process these models do not explicitly take into account. As shown in our paper, it is one of the major processes that prevent PV homogenization. Without these two processes, we cannot obtain a realistic equilibrium state in the boundary layer.

In this study, we assumed a fixed surface temperature, which may not be a good assumption for a land surface. When coupled with an underlying surface with interactive surface temperature, how the vertical thermal diffusion and surface heat flux influence the eddy equilibration is a topic we will investigate in a future study. In the real atmosphere, the boundary layer diffusion, besides being influenced by the turbulent kinetic energy, is influenced by the lower-level static stability. In addition, the depth of the boundary layer (discussed in appendix C) has large variations over ocean and land. The land surface is also characterized by a strong diurnal cycle. How these factors affect our results still needs study.

Our analysis of the Lorenz energy cycle in the standard run demonstrated that during the evolution and the maintenance of the equilibrium states, boundary layer frictional dissipation is the major sink of EKE. Boundary layer thermal diffusion and the diabatic forcing all act to remove EPE, with the latter contribution being smaller. We note that in some early observational studies (Oort and Peixoto 1983; Peixoto and Oort 1992) the sum of these two terms (usually estimated as a residual term from the energy tendency equation) was found to be a generation term for EPE. A plausible source for EPE that is omitted in our model is the release of latent heat. This indicates the limitations of dry simulations as well as the commonly used Newtonian cooling parameterization, and suggests that a more physical parameterization of the radiative–convective forcing might be needed.

Acknowledgments. This research was supported in part by the Office of Science (BER), U.S. Dept. of Energy, Grant DE-FG02-93ER61677, and in part by the Goddard Institute for Space Studies, under NASA Cooperative Agreement NNG04GF12A.

APPENDIX A

Model Description

In our β-plane multilevel quasigeostrophic model, the variables are defined in gridpoint space. The horizontal resolution of the model is 330 km in both zonal and meridional directions. The model has 17 equally spaced levels. As shown by Solomon and Stone (2001a), this resolution is good enough to simulate the model dynamics.[A1] In addition, an FFT filter is used on the streamfunction to remove the smallest-scale eddies.

a. Governing equations

In this model, the potential vorticity equation, including diabatic heating and boundary layer dissipation, is integrated:

$$\frac{\partial q}{\partial t} = -J(\psi, q) - f_o \frac{\partial}{\partial p} \frac{QR}{spC_p} + \mathbf{k} \cdot \nabla \times \mathbf{F},$$

[A1] We also tested our results in section 3d by doubling the horizontal resolution; we found, comparing with the results obtained with the original resolution for the standard run and stronger surface friction run, that the temperature and PV structure are virtually identical at the higher resolution. For the weaker surface friction run, the PV gradient in the double resolution run is slightly better homogenized (the difference around the boundary layer is less than 0.5 β). However, the nonmonotonic response of the equilibrium state PV, as well as temperature gradient to the surface friction and the mechanism we discussed in the paper, still holds.

where p is the pressure, f_o is the Coriolis parameter at the center of the channel, R is the ideal gas constant, C_p is the specific heat of the air, s is the static stability parameter, and ψ is the geostrophic streamfunction; also, $\mathbf{F}$ denotes the frictional dissipation and the heating term Q has two contributors: diabatic heating Q_r and the thermal diffusion in the boundary layer Q_d. Potential vorticity $q = \nabla^2\psi + \beta y + (\partial/\partial p)(f_o^2/s)(\partial\psi/\partial p)$.

One important difference between this model and traditional QG models is that the horizontally averaged potential temperature and static stability, instead of being specified, are allowed to evolve with time according to the equation

$$\frac{\partial}{\partial t}\overline{\theta}^{xy} = -\frac{\partial}{\partial p}\overline{\omega^*\theta^*}^{xy} + \frac{\overline{Q_r + Q_d}^{xy}}{c_p}\left(\frac{p_o}{p}\right)^{R/c_p}, \qquad \text{(A1)}$$

where p_o is the pressure at the surface, the overbar and xy superscript indicate the horizontally averaged quantity, and the superscript * indicates the eddy component of the variable. This tendency equation is derived from the horizontally averaged thermodynamic equation and is exact except that the heating associated with the vertical heat flux by the zonal mean flow is neglected. As shown by Gutowski (1983), this is a reasonable approximation in midlatitudes. Thus, in our model, the thermal stratification is maintained by the vertical eddy heat flux and the diabatic heating in the free atmosphere and by the vertical eddy heat flux, diabatic heating, and thermal diffusion in the boundary layer. As shown by Gutowski (1985), the interaction between the vertical eddy heat flux and the stratification, which is neglected in conventional QG theory, plays an important role in baroclinic adjustment. Because we still use horizontal uniform stratification, adding Eq. (A1) does not break the QG scaling. In addition, in the quasi-equilibrium state, where the stratification has tiny variations with time, the model behavior is similar to the traditional QG model with time-invariant stratification, which has been confirmed by Solomon and Stone (2001a) and by Zurita-Gotor and Vallis (2009).

b. Diabatic heating

Diabatic heating in this model is parameterized by the Newtonian cooling form:

$$Q_r = c_p\frac{T_e - T}{\tau_r}, \qquad \text{(A2)}$$

where T_e is the atmospheric temperature in the RCE state corresponding to the specified surface temperature and τ_r (= 40 days) is the relaxation time scale. The globally averaged surface temperature in our model is set to be 280 K, and the lapse rate $d\overline{T_e}^{xy}/dz$ of the RCE state is chosen to be -7 K km^{-1} in the troposphere and zero in the stratosphere. The meridional variation of the potential temperature of the RCE state in the troposphere is set so that over the central half of the channel, for $1/4L \le y \le 3/4L$,

$$\theta_e^\dagger(y,p) = -21.5\sin\left[\frac{\pi(y - L/2)}{L/2}\right], \qquad \text{(A3)}$$

where $\theta_e^\dagger = \theta_e - \overline{\theta_e}^{xy}$, L is the width of the channel, and there is no meridional temperature gradient in the regions $0 \le y \le 1/4L$ and $3/4L \le y \le L$. Thus, the temperature difference over the channel is 43 K, which approximates the equator-to-pole surface temperature difference in winter in the Northern Hemisphere. In the stratosphere, the potential temperature gradient of the RCE state is one tenth of that in the troposphere and of the opposite sign. The RCE state is also taken as the initial state in this study.

c. Thermal diffusion in the boundary layer

The surface heat exchange between atmosphere and ocean is represented by the linearized bulk aerodynamic drag formula:

$$F_{sh} = -C_{dt}c_p\rho_s(\theta_{\text{air}} - \theta_{\text{sea}}), \qquad \text{(A4)}$$

where $C_{dt} = C_{\text{surface}}|\mathbf{v_s}|$ is the drag coefficient and ρ_s is the surface air density. In this study, C_{dt} is chosen to be constant, and 0.03 m s^{-1} is taken as its standard value. The sea surface potential temperature θ_{sea} is kept fixed, which is the RCE state surface potential temperature. We assume that the first model level is a well-mixed layer so that the surface air potential temperature θ_{air} is equal to the potential temperature at the first level, which is 32 hPa above the surface.

Above the surface, the vertical turbulent heat flux in the boundary layer is parameterized in the diffusive form:

$$F_{sh} = \nu_S(p)c_p\rho^2 g\frac{\partial\theta}{\partial p}, \qquad \text{(A5)}$$

where g is the acceleration due to gravity and where, in the standard run, the vertical distribution of the diffusion coefficient is

$$\nu_S(p) = \mu_s\left(\frac{p}{p_o}\right)^3 \text{m}^2\ \text{s}^{-1}, \qquad \text{(A6)}$$

and 5 m^2 s^{-1} is taken to be the standard value for μ_s. Heating by thermal diffusion is calculated from the heat flux:

$$Q_d = g\left(\frac{p}{p_o}\right)^{R/c_p}\frac{\partial F_{sh}}{\partial p}. \qquad \text{(A7)}$$

Here we want to point out that because of the vertical turbulent heat transport, the stratification in the boundary layer can be weak. However, this merely means that the vertical temperature advection by the flow is small and the horizontal temperature advection in this case is dominant. Thus, the QG scaling still holds.

d. Frictional dissipation in the boundary layer

The parameterization of friction is analogous to thermal diffusion, $\mathbf{F} = g\,\partial\tau_m/\partial p$, where τ_m is the shear stress and is parameterized by a linearized bulk aerodynamic drag at the surface and vertical diffusion in the boundary layer (BL):

$$\boldsymbol{\tau}_\mathbf{m} = -C_{df}\rho_s\mathbf{v}\ \text{(surface)} \quad \text{and} \tag{A8}$$

$$\boldsymbol{\tau}_\mathbf{m} = \nu_M(p)\rho^2 g\frac{\partial\mathbf{v}}{\partial p}\ \text{(BL)}, \tag{A9}$$

where $\mathbf{v} = (-\psi_y, \psi_x) = (u_g, v_g)$ and

$$\nu_M(p) = \mu_m\left(\frac{p}{p_o}\right)^3 \text{m}^2\ \text{s}^{-1}. \tag{A10}$$

In the standard run, $\mu_m = 5\ \text{m}^2\ \text{s}^{-1}$ and C_{df} is still chosen to be 0.03 m s^{-1}. In section 3, only the shear stress by geostrophic component is considered.[A2]

APPENDIX B

Spectral Distribution of Eddy Heat Flux and Critical Layer Evolution

Using the same method as Randel and Held (1991), we calculate the equilibrium state zonal wavenumber–phase speed covariance spectra of $[v^*T^*]$ at 875 hPa at the center of the channel for the standard run and $C_{df} = 0.01$ m s^{-1} run. As shown in Fig. B1, our model has a simple spectral distribution in the equilibrium state, which is consistent with the fact that the maintenance of the equilibrium state is dominated by the wave–mean flow interaction. In the standard run, most of the lower-level eddy heat flux comes from wavenumber 6 with phase speed around 8 m s^{-1}, whose magnitude is almost 10 times bigger than adjacent wavenumbers. With weaker surface friction, almost all the eddy heat flux comes from wavenumber 4 with phase speed around 4 m s^{-1}. Even though there is still a minor peak in wavenumber 6 with phase speed around 11 m s^{-1}, its contribution is much smaller than wavenumber 4. Thus, in section 3 we only plot $U - C_r$ for the dominant waves.

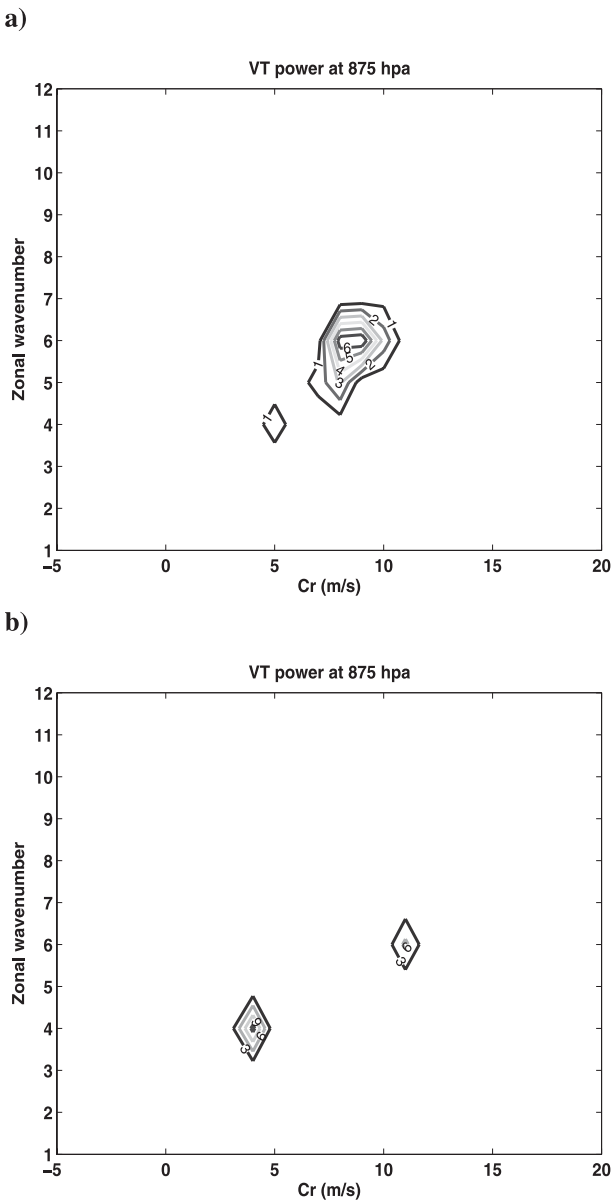

FIG. B1. Zonal wavenumber–phase speed covariance spectra of $[v^*T^*]$ at 875 hPa at the center of the channel for the (a) SD run and (b) $C_{df} = 0.01$ m s^{-1} run. The contour interval is 1 K m s^{-1} ΔC_r^{-1} for the SD run and 3 K m s^{-1} ΔC_r^{-1} for $C_{df} = 0.01$ m s^{-1} run (the zero contour is not plotted), where the unit phase speed interval is 1.0 m s^{-1}.

As displayed in Fig. 1, our equilibrium state is not a totally steady state. Besides showing the statistical distribution of $U - C_r$ in the equilibrium state, in Fig. B2 we also show the evolution of $U - C_r$ of the dominant waves at the center of the channel for the standard and weaker surface friction run. We find in the equilibrium

[A2] We tested our results in section 3d by including the influence of ageostrophic winds in the shear stress in the boundary layer and found that despite quantitative differences the nonmonotonic response of the PV gradient to the surface friction is basically the same.

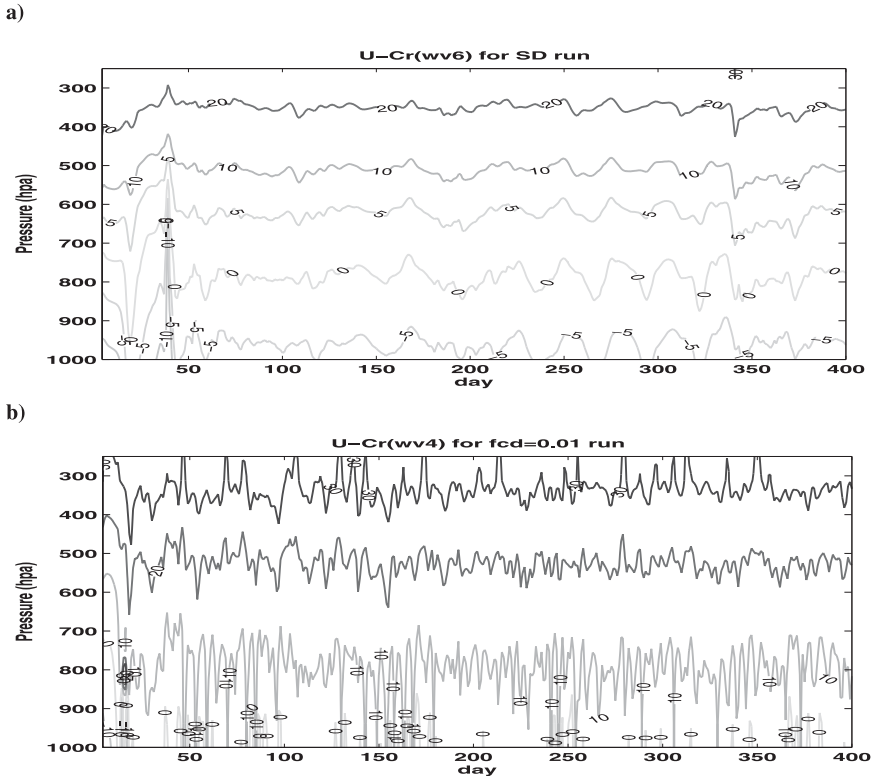

FIG. B2. Evolution of intrinsic phase speed ($U - C_r$) of the dominant wave at the central of the channel in the first 400 days for the (a) standard and (b) C_{df} = 0.01 m s^{-1} runs.

state that the critical layer in the standard run varies from 750 to 850 hPa. Under weaker surface friction, the critical layer at the center of the channel disappears most of the time, and at 875 hPa, $U - C_r$ is always positive, which confirms our statistical results.

APPENDIX C

How the Results Depend on the Depth of the Boundary Layer

In this section, we study how the depth of boundary layer affects our results. We use four different thermal diffusion and momentum dissipation profiles to compare with the standard run: $\nu(p) = \mu[(p - p_{\mathrm{b1}})/(p_0 - p_{\mathrm{b1}})]^3$ m^2 s^{-1} for levels below p_{bl} and $\nu(p) = 0$ for levels above it. In this expression, p_{bl} is the pressure at the boundary layer and p_o is the pressure at the surface; p_{bl} = 1000, 850, 700, and 500 hPa, respectively (p_{bl} = 1000 hPa is the case where vertical thermal diffusion and momentum dissipation are not considered).

Without boundary layer diffusion, as shown by Figs. C1a,c,e,g, the mean field and eddy heat flux distributions are similar to the Snu0 run (where thermal diffusion is zero), which confirms our conclusion that boundary layer momentum dissipation has very little effect on the equilibrium state. This also indicates that the influence of the boundary layer depth is primarily associated with the vertical thermal diffusion. From Fig. C1g, we find that the response of the eddy heat flux is similar to that in the Snu runs—that is, deeper boundary layer diffusion results in stronger eddy heat flux. For the mean fields, the free troposphere PV gradient is also similar to the Snu runs. The PV gradient is homogenized over a deeper layer when the boundary layer is shallower. However, the response of the mean temperature gradient and stratification is more complicated. As the boundary layer becomes shallower, the temperature gradient distribution is closer to the zero boundary layer diffusion run. From Fig. C1c, the distribution of the static stability is sensitive to the diffusion profile. For p_{bl} = 500, 700 hPa, the response of $d\overline{\theta}^{xy}/dz$ is also similar to the Snu runs. Under deeper boundary layer diffusion, the lower-level stabilization is more efficiently prevented. However, when the boundary layer becomes shallow, where p_{bl} = 850 hPa, $d\overline{\theta}^{xy}/dz$ above 850 hPa is similar to the state without boundary layer diffusion but strongly stabilized at 875 hPa.

Even though the depth of boundary layer can influence the equilibrium state, we find that with different

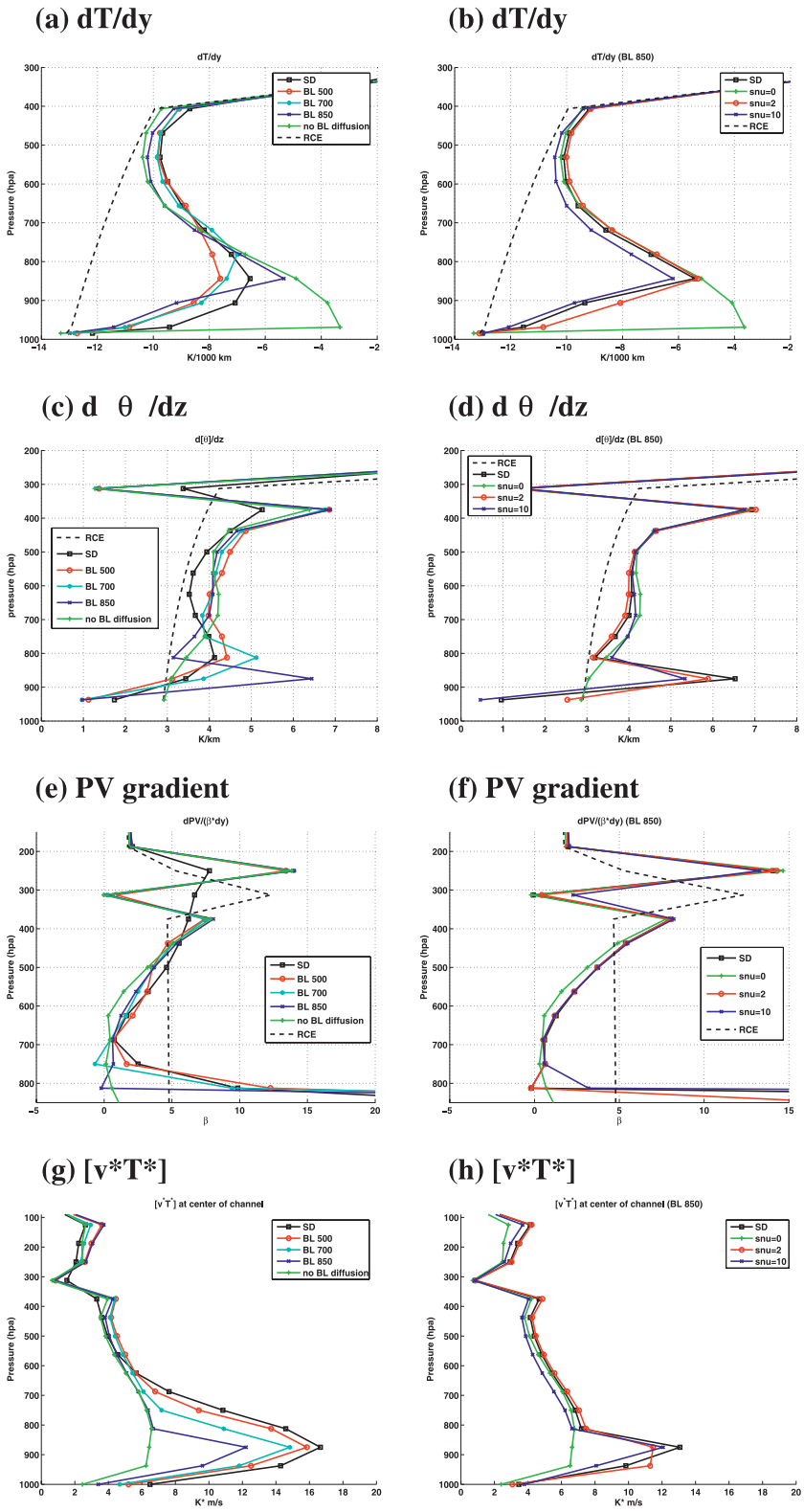

FIG. C1. Comparison of equilibrated state zonal mean (a) dT/dy at the center of the channel, (c) $d\overline{\theta}^{xy}/dz$, (e) $dPV/(\beta dy)$ and (g) meridional eddy heat flux at the center of the channel for different p_{bl}. (b),(d),(f),(h) As in (a),(c),(e), and (h) respectively, but for different μ_s when $p_{\mathrm{bl}} = 850$ hPa.

boundary layer depths, the response of the flow to different boundary layer processes is similar to that in section 3. For example, if we use the p_{bl} = 500 hPa profile and do the same experiments as in section 3, the equilibrium states illustrate the same tendencies to the boundary layer processes. However, as the boundary layer becomes shallower, our model has little sensitivity to the strength of boundary layer thermal diffusion and surface heat flux. As shown in Figs. C1b,d,f,h, when p_{bl} = 850 hPa, the equilibrium state is almost insensitive to μ_s when μ_s is nonzero. However, without thermal diffusion, there are still large variations in eddy heat fluxes as well as the temperature gradient. Even with a shallow boundary layer, including these two boundary layer processes is still important in simulating the real atmosphere.

REFERENCES

Branscome, L. E., W. J. Gutowski, and D. Stewart, 1989: Effect of surface fluxes on the nonlinear development of baroclinic waves. *J. Atmos. Sci.,* **46,** 460–475.

Card, P. A., and A. Barcilon, 1982: The Charney stability problem with a lower Ekman layer. *J. Atmos. Sci.,* **39,** 2128–2137.

Cehelsky, P., and K. K. Tung, 1991: Nonlinear baroclinic adjustment. *J. Atmos. Sci.,* **48,** 1930–1947.

Chen, G., I. Held, and W. Robinson, 2007: Sensitivity of the latitude of the surface westerlies to surface friction. *J. Atmos. Sci.,* **64,** 2899–2915.

Gall, R., 1976: A comparison of linear baroclinic instability theory with the eddy statistics of a general circulation model. *J. Atmos. Sci.,* **33,** 349–373.

Gutowski, W. J., 1983: Vertical eddy heat fluxes and the temperature structure of the mid-latitude troposphere. Ph.D. thesis, Massachusetts Institute of Technology, 294 pp.

——, 1985: Baroclinic adjustment and the midlatitude temperature profiles. *J. Atmos. Sci.,* **42,** 1733–1745.

Held, I., and M. Suarez, 1994: A proposal for the intercomparison of the dynamical cores of atmospheric general circulation models. *Bull. Amer. Meteor. Soc.,* **75,** 1825–1830.

Holton, J. R., 2004: *An Introduction to Dynamic Meteorology*. 4th ed. Elsevier, 535 pp.

James, I. N., 1987: Suppression of baroclinic instability in horizontally sheared flows. *J. Atmos. Sci.,* **44,** 3710–3720.

——, and L. J. Gray, 1986: Concerning the effect of surface drag on the circulation of a baroclinic planetary atmosphere. *Quart. J. Roy. Meteor. Soc.,* **112,** 1231–1250.

Kirk-Davidoff, D., and R. Lindzen, 2000: An energy balance model based on potential vorticity homogenization. *J. Climate,* **13,** 431–448.

Lindzen, R. S., 1993: Baroclinic neutrality and the tropopause. *J. Atmos. Sci.,* **50,** 1148–1151.

——, and J. Barker, 1985: Instability and wave over-reflection in stably stratified shear flow. *J. Fluid Mech.,* **151,** 189–217.

Oort, A. H., and J. P. Peixoto, 1983: Global angular momentum and energy balance requirements from observations. *Advances in Geophysics*, Vol. 25, Academic Press, 355–490.

Peixoto, J. P., and A. H. Oort, 1992: *Physics of Climate*. Springer-Verlag, 520 pp.

Randel, W. J., and I. M. Held, 1991: Phase speed spectra of transient eddy fluxes and critical layer absorption. *J. Atmos. Sci.,* **48,** 688–697.

Robinson, W. A., 1997: Dissipation dependence of the jet latitude. *J. Climate,* **10,** 176–182.

Schneider, T., 2004: The tropopause and the thermal stratification in the extratropics of a dry atmosphere. *J. Atmos. Sci.,* **61,** 1317–1340.

Simmons, A. J., and B. J. Hoskins, 1978: The life cycles of some nonlinear baroclinic waves. *J. Atmos. Sci.,* **35,** 414–432.

Solomon, A. B., 1997a: An observational study of the spatial and temporal scales of transient eddy sensible heat fluxes. *J. Climate,* **10,** 508–520.

——, 1997b: The role of large-scale eddies in the nonlinear equilibration of a multi-level model of the mid-latitude troposphere. Ph.D. thesis, Massachusetts Institute of Technology, 234 pp.

——, and P. H. Stone, 2001a: Equilibration in an eddy-resolving model with simplified physics. *J. Atmos. Sci.,* **58,** 561–574.

——, and ——, 2001b: The sensitivity of an intermediate model of the midlatitude troposphere's equilibrium to changes in radiative forcing. *J. Atmos. Sci.,* **58,** 2395–2410.

Stone, P. H., 1978: Baroclinic adjustment. *J. Atmos. Sci.,* **35,** 561–571.

——, and B. Nemet, 1996: Baroclinic adjustment: A comparison between theory, observations, and models. *J. Atmos. Sci.,* **53,** 1663–1674.

Swanson, K., and R. T. Pierrehumbert, 1997: Lower-tropospheric heat transport in the Pacific storm track. *J. Atmos. Sci.,* **54,** 1533–1543.

Valdes, P. J., and B. Hoskins, 1988: Baroclinic instability of the zonally averaged flow with boundary layer damping. *J. Atmos. Sci.,* **45,** 1584–1593.

Zurita, P., and R. Lindzen, 2001: The equilibration of short Charney waves: Implications for potential vorticity homogenization in the extratropical troposphere. *J. Atmos. Sci.,* **58,** 3443–3462.

Zurita-Gotor, P., and R. Lindzen, 2004: Baroclinic equilibration and the maintenance of the momentum balance. Part II: 3D results. *J. Atmos. Sci.,* **61,** 1483–1499.

——, and ——, 2007: Theories of baroclinic adjustment and eddy equilibration. *The Global Circulation of the Atmosphere: Phenomena, Theory, Challenges*, T. Schneider and A. Sobel, Eds., Princeton University Press, 22–46.

——, and G. Vallis, 2009: Equilibration of baroclinic turbulence in primitive equation and quasi-geostrophic models. *J. Atmos. Sci.,* **66,** 837–863.